Effect of H2S and HCl contaminants on nickel and ceria pattern anode solid oxide fuel cells

Tabish, A. N.; Patel, H. C.; Mani, A.; Schoonman, J.; Aravind, P. V.

Published in:
Electrochimica Acta

DOI:
10.1016/j.electacta.2022.140592

Publication date:
2022

Electrochimica Acta 423 (2022) 140592

Contents lists available at ScienceDirect

Electrochimica Acta

journal homepage: www.journals.elsevier.com/electrochimica-acta

Effect of H_2S and HCl contaminants on nickel and ceria pattern anode solid oxide fuel cells

A.N. Tabish [a,b,*], H.C. Patel [a,c], A. Mani [d], J. Schoonman [e], P.V. Aravind [a,f]

[a] Department of Process and Energy, Delft University of Technology, Delft, CA 2628, the Netherlands
[b] Department of Chemical Engineering, UET Lahore (New Campus), Bypass, Lahore 39021, Pakistan
[c] SBM Offshore, Schiedam 3115 JD, the Netherlands
[d] Energy Academy Europe (ESRIG), Nijenborgh 6 AG, Groningen 9747, the Netherlands
[e] Department of Chemical Engineering, Section Materials for Energy Conversion and Storage, Delft University of Technology, the Netherlands
[f] Energy and Sustainability Research Institute Groningen, University of Groningen, Groningen, AB 9700, the Netherlands

ARTICLE INFO

Keywords:
SOFC poisoning
H_2S
HCl
Pattern anode
Ceria

ABSTRACT

In this study, with the motivation of elucidating the effect of H_2S and HCl on solid oxide fuel cell anodes, nickel and ceria pattern anodes are prepared on yttrium-stabilized zirconia electrolyte, and the effect of H_2S and HCl on their performance is tested using electrochemical impedance spectroscopy. However, it has been found that while H_2S adversely impacts both nickel and ceria, the poisoning caused is reversible for nickel and only partially reversible for ceria. Poisoning kinetics are similar and fast for both materials, while recovery kinetics are slower for ceria than nickel. High sulfur coverage is the rate-limiting factor inferred from the elementary kinetic modeling. Unlike H_2S, the presence of HCl appeared to be favorable for electrochemical oxidation as the polarization resistance of both pattern electrode cells decreased upon feeding HCl contaminated hydrogen gas. Similar behavior has not been reported previously, and the conclusion regarding underlying mechanisms requires further investigation.

1. Introduction

Solid oxide fuel cell (SOFC) offers a great prospect for the most efficient utilization of various fuels. The hydrocarbon fuels suitable for SOFC applications, i.e., natural gas, biogas, and syngas, contain significant quantities of H_2S and HCl impurities that can potentially poison the anode material and degrade the cell performance [1,2]. Lohsoontorn et al. [3] have reported the thermodynamic predictions of H_2S interactions with nickel and ceria under SOFC operating conditions. Numerous experimental studies have also been conducted to determine the effect of H_2S on SOFC anodes at values up to 1000 ppm. It has been found that the polarization resistance increases with increasing concentration, temperature, and microstructure, among other factors [4–6]. It is envisaged that even very low concentrations of H_2S (as low as 0.05 ppm at 1073 K) will have a detrimental effect on the performance of the cells when used for an extended period of time [7]. The H_2S-related performance degradation of Ni/YSZ-based cells can occur in three consecutive phases, as suggested by Chen et al. [8]. A rapid initial performance loss is followed by either (i) no further loss, (ii) a slow performance loss followed by steady-state behavior, or (iii) a continuous performance loss without stabilization. It is commonly believed that the sulfur adsorbs at the nickel surface sites or the TPB lead to an initial rapid and reversible performance loss [9–12].

Additionally, the poisoning effect of HCl and other chlorine compounds such as Cl_2 and CH_3Cl has been studied at concentrations ranging from 1 part per million to 1000 parts per million. The pertinent literature reveals several key observations, including the following:

(1) The effect of HCl on cell performance is negligible up to 50 ppm HCl [13–15]
(2) High concentrations may result in reversible [16,17] as well as irreversible performance losses [18]
(3) Increased temperature results in a decrease in HCl-related degradations [17]
(4) Electrolyte-supported cells (ESC) are more sensitive to HCl than anode-supported cells (ASC) [18]

Most of these studies rule out nickel chlorination (formation of

* Corresponding author at: Department of Chemical Engineering, UET Lahore (New Campus), Bypass, Lahore 39021, Pakistan
E-mail address: antabish@uet.edu.pk (A.N. Tabish).

https://doi.org/10.1016/j.electacta.2022.140592
Received 1 November 2021; Received in revised form 13 April 2022; Accepted 18 May 2022
Available online 20 May 2022

$NiCl_2$) as a major cause of performance loss, but the adsorption of Cl species on the nickel surface has been implicated in almost all of the studies.

Ni/YSZ is a state-of-the-art anode material, and its interaction chemistry with various fuel components, including contaminants, is better understood. It is considered that Ni/YSZ degrades at an accelerated rate in practical fuel environments. In the search for a stable anode material, various strategies have been proposed, including replacing nickel with another metal such as Copper [19,20], Tungsten [21], and Molybdenum. Additionally, the ceramic phase can be substituted with a Mixed Ionic Electronic Conductor (MIEC), such as ceria or other perovskite materials, to improve the performance of the fuel cell [22]. Anode sulfur tolerance of Ni-YSZ anodes can be significantly improved by optimizing their microstructure and SOFC operating conditions [23, 24]. Among MIEC electrodes, the composite of nickel and gadolinium-doped ceria (Ni/GDC) is considered a potential alternative to Ni/YSZ, and it outperforms the latter even under stringent conditions. Ni/GDC exhibits significantly different and more favorable interaction chemistry between the anode and fuel components than Ni/YSZ due to the MIEC nature of ceria in the anode. However, despite many studies with ceria-based electrodes, the knowledge of electrode electrochemistry is limited and inconclusive. Therefore, extensive work with ceria and ceria-based anode materials is required to develop future electrodes.

For non-electrochemical applications, ceria-based materials have proven effectiveness as desulfurization sorbent for gas cleaning [25–27]. Reduced ceria is expected to be a better adsorbent for H_2S than the corresponding oxidized form. While the exact kinetics of the chemisorption remain unknown, even elemental sulfur can form during the desorption step [10,21]. From the catalysis literature, we know that ceria is an excellent catalyst for the oxidation of HCl at temperatures ranging from 350 to 450 ℃ in the presence of an excess amount of oxygen [28]. Because of the presence of adequate oxygen, ceria preserves its catalytic activity. While it is envisaged that the concentration of HCl in practical fuels will be in the ppm range, the catalytic activity of ceria-based anodes may be affected because of the reducing conditions in the anode chamber. Jeanmonod et al. [29] have reported performance loss even with 5 ppm(v) HCl while operating under polarization in the solid oxide electrolysis cell.

When compared to nickel as a fuel cell anode material, the effect of H_2S and HCl on ceria has been the topic of far fewer experimental studies. Ceria is expected to be poisoned by sulfur, but no conclusive evidence has been found to indicate which species is responsible [3,20, 30,31,32], even though studies have pointed toward a cerium oxysulfide phase on exposure to H_2S [21]. According to the gas cleaning literature, sulfides form on ceria rather than nickel, and there is a consensus that no bulk sulfides form at SOFC operating conditions with a few ppm of H_2S. For instance, it is common practice to employ CuO_2-CeO_2 in the H_2S cleaning process since it is believed that the oxygen-storing capabilities of ceria will aid in keeping the CuO_2 in an oxidized state [20].

It is vital to research the effects of fuel impurities on nickel and ceria individually and then evaluate the performance of the two anodes under SOFC operating conditions because Ni/GDC anodes, a composite of nickel and ceria, are believed to be a feasible alternative to Ni/YSZ anodes. Such a comparison may also be helpful in studying and designing the modified Ni/YSZ electrodes - for instance, ceria infiltration has shown improved sulfur tolerance of conventional Ni/YSZ electrodes. Cermet anodes are not ideal for studying the reaction kinetics with electrochemical impedance spectroscopy (EIS), as non-TPB processes can dominate over electrochemistry. For example, the gas diffusion impedance can be significantly higher in cermet anodes than the charge transfer resistance [33]. Because this study aims to investigate the oxidation kinetics and the influence of fuel contaminants on the anode performance, any impacts coming from geometrical parameters must be avoided as far as possible. Because of this, we use pattern anode cells, which have a well-defined topology and allow for localization of the reactions. Also, because the current drawn is so small, it is not envisaged that the gas diffusion impedance will significantly impact the response time [35]. The impedance spectra are also easier to analyze. In previous works, we have used nickel and ceria pattern electrode cells to analyze the oxidation of hydrogen and carbon monoxide and mixtures thereof and highlighted the possible use of (un)doped ceria as an anode material in its reduced state [34,35]. Combined with modeling, this has proved to be a useful exercise in understanding the differences in the oxidation mechanism between nickel and ceria and, indeed, proposed possible reaction schemes [5,36,37]. Further, we derived TPB-based kinetics from the pattern electrode cell experimental data and proposed a procedure for implementing such kinetic information in the computational fluid dynamic model [38,39].

Pattern electrode cells made of nickel and ceria are used in this study to examine the performance of these materials when exposed to sulfur and chlorine contaminants under SOFC conditions. The use of pattern electrode cells can aid in the quantification of poisoning effects, as well as the determination of the relative kinetics of these anode materials. With knowledge of nickel and ceria poisoning effects obtained from pattern electrode cell investigations, it would be possible to conclude the poisoning of commercial cells. Previous studies have focused only on nickel pattern electrode cells on YSZ substrates [40]. This comparison of nickel and ceria, on the other hand, has not been done previously. Further, an elementary kinetic model is developed to capture and quantify the effect of sulfur poisoning on the ceria pattern electrode cells.

2. Experimental

This study uses nickel and ceria pattern electrode cells prepared on a YSZ substrate. Symmetrical cell configuration was chosen to study the anode processes. 8 % Yttria-stabilized zirconia (YSZ) substrates (25 mm diameter and 250 μm thick) were obtained from Fuel Cell Materials (www.fuelcellmaterials.com). YSZ disks were placed in a stainless-steel mask, designed in-house with the desired pattern. Target electrode materials were then sputtered by DC magnetron sputtering to prepare symmetrical nickel and ceria pattern electrodes cell. The deposition rate of 0.12 nm/s and 0.035 nm/s and thickness of 1780 nm and 500 nm were achieved for nickel and ceria, respectively. The resultant pattern electrode cell dimensions and test assembly are shown in Fig. 1.

For effective current collection, a square gold mesh (1024 mesh/cm^2) was used on both cell sides. The cell, sandwiched between two ceramic supports, was placed inside the tubular furnace for electrochemical testing. The electrochemical impedance spectroscopy (EIS) was performed at temperatures ranging from 750 to 850 ℃ using a Gamry potentiostat (Reference 600). Sinusoidal perturbation of 15 mV and frequency range of 100–0.05 Hz (12 points/decade) was maintained for all EIS measurements. The AC perturbation was applied without any biasing, making the cell operation superficially at equilibrium. Due to the symmetrical nature of the cell and the single gas atmosphere, the reference electrode was combined with the counter electrode for EIS measurements. The following sequence of operating conditions was maintained for measurements.

1 The furnace was heated to a higher temperature (850 ℃ in this case) at a ramp rate of 40 ℃/h. Cells were flushed with 100 ml/min of nitrogen gas during the heating phase.
2 Once 850 ℃ temperature was attained, the gas was gradually switched from inert to wet hydrogen (3 vol % hydrogen) at 100 ml/min. The moisture was added using a high-precision syringe pump. The EIS spectra were recorded at an interval of at least one hour, and the pattern of cell stabilization was keenly observed. It took more than 24 h for both nickel and ceria pattern electrode cells to obtain a stable and consistent spectrum. This testing phase was attributed to the cells' initial thermal and electrochemical treatment.
3 A mixed stream of hydrogen and H_2S was then added to the wet hydrogen steam while keeping the total flow (100 ml/min) the same.

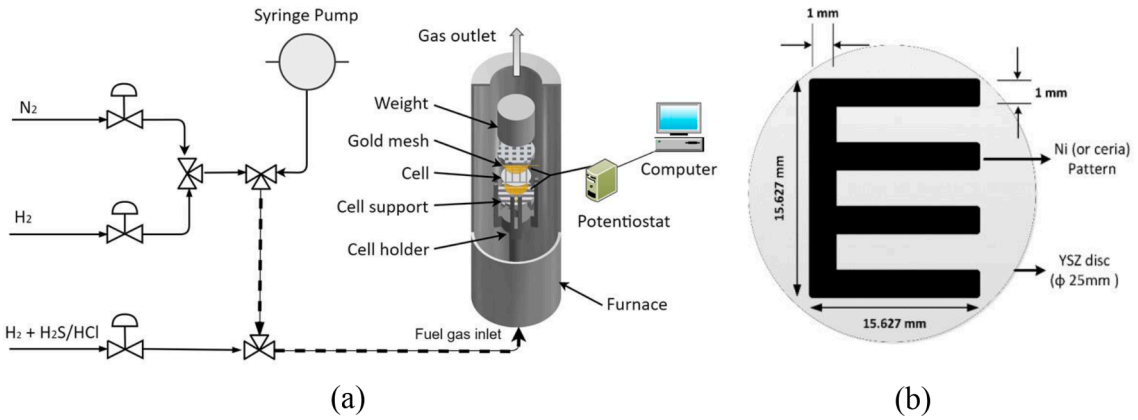

Fig. 1. Experimental setup. (a) Electrochemical test assembly and (b) schematic of the pattern electrode cell. The cell, with gold mesh acting as a current collector, was held between the two ceramic supports.

EIS measurements were carried out at H_2S concentrations of 5 ppm (v) and 20 ppm(v). An exposure time of at least 6 h was maintained for each concentration.

4 To recover the cell from poisoning effects, the contaminant-free gas (wet hydrogen) was introduced for at least 20 h. The furnace temperature was then lowered to study the effect of H_2S poisoning at a lower temperature.

5 The same procedure was followed for studying the effect of HCl (60 ppm(v) and 150 ppm(v)) contaminants. An exposure time of at least 6 h was maintained for each concentration. We also tested Ni/GDC cermet cells with HCl (up to 300 ppm) for literature comparison.

3. Results and discussion

3.1. Effect of H_2S contaminant on nickel and ceria cells

3.1.1. Effect of H_2S on cell performance

Fig. 2 shows the impedance spectra for nickel and ceria pattern electrode cells before H_2S exposure, with H_2S, and after removal (i.e., with humidified H_2). Corresponding Bode plots are given in the supplementary material (Figs. S1 and S2). The spectra with 5 ppm are not shown for brevity, but the polarization resistance is discussed in detail for ceria.

As can be observed from Fig. 2a, the polarization resistance of the nickel pattern electrode cell increases by a factor of 1.4 at 850 ℃ upon feeding H_2S contaminated gas to the fuel cell. Further, the impedance spectra before exposure to H_2S and after its removal completely overlap, which is true for all the temperatures tested in this study. This finding is consistent according to prior investigations on nickel cermet anodes, which have been proven to cause completely reversible cell poisoning at low H_2S concentrations. According to previous research on cermet anodes, which has mostly focused on Ni-YSZ composites, the poisoning could be caused by the dissociative adsorption of sulfur species on nickel [8,41,42]. When sulfur atoms attach to the surface of nickel, they block the surface reaction sites that would otherwise be available for hydrogen adsorption and oxidation via electrochemical means. The adsorbed sulfur may also chemically react with nickel particles, leading to surface modification and performance loss, as proposed by Cheng and Liu [43]. Lussier et al. [44] proposed that H_2S can lead to nickel depletion due to migration, thereby compromising the percolated network and cell performance. The permanent loss may result from short exposure to high H_2S concentration or prolonged exposure to low H_2S concentration.

Like nickel, ceria also suffers serious performance loss upon H_2S exposure. However, at least for the time (>20 h) investigated in this study, this loss is not totally reversible. The trend has been observed for all temperatures tested in this study, as shown in the supplementary material (Fig. S3). Mirfakhraei et al. [45] tested GDC electrodes in a 10 ppm H_2S environment and observed ca. 50 % increase in the polarization resistance in 1 h and ca. 90 % recovery in 3 h. In the same study, they observed only a 5.5 % increase in the polarization resistance of nickel infiltrated GDC electrodes after 24 h of operation, followed by complete recovery. The authors believed that sulfur preferentially adsorbed on the infiltrated nickel surface, and ceria supplied the oxide ions to adjacent nickel, oxidizing the adsorbed sulfur and keeping it clean for hydrogen adsorption. Full recovery of Ni/GDC electrode after considerable poisoning at 20 ppm H_2S has also been reported elsewhere [46]. Further, the effect of operating temperature on the increment of the polarization resistance at 5 ppm and 20 ppm H_2S concentration is shown in Fig. 3. It appears that increasing operating temperature lowers the H_2S poisoning at 5 ppm concentration which is not the case at 20

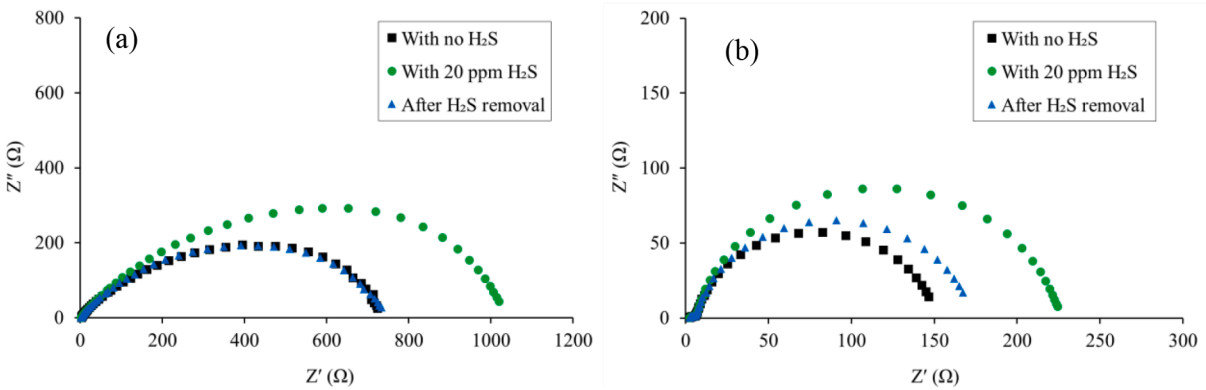

Fig. 2. Impedance spectra of H_2S contamination of pattern electrode cells of nickel (a) and ceria (b) at 850 ℃.

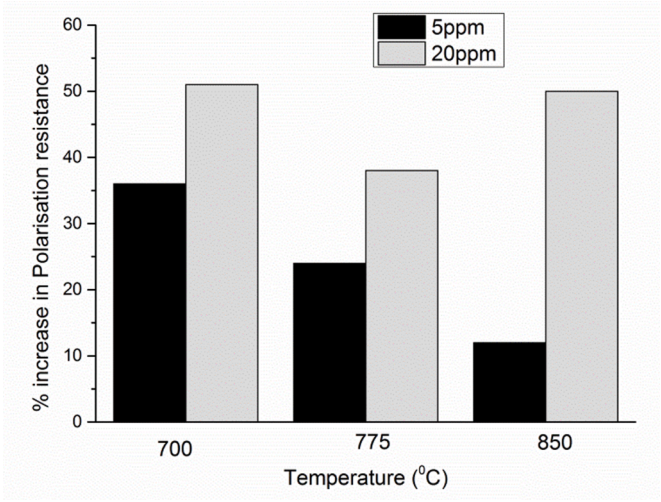

Fig. 3. The effect of operating temperature on H_2S poisoning of ceria pattern electrode cells at two different concentration levels (5 ppm and 20 ppm).

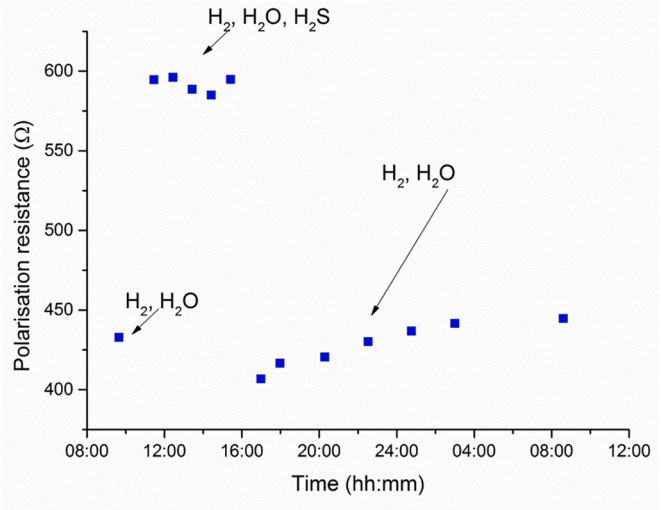

Fig. 4. Stabilization time for ceria pattern electrode cells during and after poisoning with 20 ppm H_2S at 775 ℃.

ppm. At 20 ppm H_2S, the performance loss due to poisoning is significantly high and independent of the operating temperature. In this work, it appeared that the ceria surface remained saturated with sulfur species at concentrations of 20 ppm for all of the temperatures examined.

From the results mentioned above, it is found that H_2S poisons both nickel and ceria. If we compare the change in the polarization resistance at 20 ppm, ceria poisoning is more severe than nickel – polarization resistance of ceria increased by 53.4 % compared to a 39.6 % increase for a nickel. Further, nickel recovery to original performance after poisoning is complete, whereas ceria recovery is only partial (about 75 % at 850 ℃) for at least the test duration of this study. This is an interesting observation for the future development of ceria-based anodes such as Ni-GDC for operation with sulfur-contaminated fuels. On the contrary, the polarization resistance with ceria, even with poisoning, is lower than nickel without poisoning (Fig. 2). As a result, it is reasonable to anticipate that a Ni/GDC cell will outperform a normal Ni/YSZ cell. The study of underlying mechanisms for electrochemical oxidation of H_2S contaminated hydrogen and syngas on Ni/GDC anode is ongoing and beyond the scope of this study.

3.1.2. *H_2S poisoning and recovery kinetics*

It is observed that nickel cells stabilize relatively quickly after the removal of H_2S, as shown for 20 ppm H_2S at 800 ℃ in the supplementary information (Fig. S4). Generally, it takes around 60 min to stabilize after removing H_2S at all temperatures. Still, the recovery is slower than the poisoning, which agrees with the literature [8,47,48]. H_2S adsorbs on nickel, according to previous research. However, no bulk sulfides are normally found at high temperatures and low concentrations [43]. A relatively high sulfur concentration or thermodynamically favored operating conditions such as low temperature are required to form nickel sulfides; however, this was not the case under the experimental conditions studied [3,49]. The reaction of H_2S with the nickel depends on the operating temperature and H_2S concentration. The sulfur poisoning is expected to become more severe with increasing concentration for a given voltage and temperature. Also, increasing temperature alleviates the poisoning effect of H_2S on the SOFC anode [7,50].

The stabilization behavior of ceria pattern electrode cells during and after poisoning with 20 ppm H_2S at 775 ℃ is shown in Fig. 4. As can be observed, the polarization resistance after H_2S removal does not recover to the pre-poisoning value, and even the time needed for stabilization is much longer than with nickel pattern electrode cells. With one exception, Mirfakhraei et al. [51] showed similar behavior for Au-GDC-YSZ anodes. The poisoning and recovery kinetics were found to be slow in their research. However, according to the current study's findings, poisoning occurs quite fast, but recovery occurs far more slowly. This was observed in gas cleaning studies, where the adsorption was very fast, and the regeneration was much slower [10]. It was attributed to the readsorption of H_2S species. The desorbed H_2S species from the bulk are readsorbed on the surface layers in this mechanism. This occurs when there is adsorption of sulfur at the surface and in layers below the surface.

3.1.3. *Discussion on H_2S poisoning mechanism*

The mechanism for the interaction between nickel and H_2S has been discussed extensively [20,44,47–49,52–54]. A two-stage process is reported where a fast degradation is observed during the first few minutes of poisoning, and then a gradual decrease in the cell performance is observed [8]. The adsorption of H_2S around the TPBs leads to a decrease in the cell's effective active area, resulting in lower performance and even breakdown. Typically, increased nickel agglomeration is observed, which results in lower performance. The irreversible performance loss is generally observed during long-term tests when the operation time exceeds several hundred hours [55]. The cell breakdown can also happen in extreme cases where nickel agglomeration is so high that percolation is lost, hence electrical connectivity. No such irreversible damage was observed in the pattern electrode cells tested in the temperature and concentrations chosen for this study. The poisoning kinetics are significantly fast in both pattern electrode cells and Ni/GDC cermet cells. The recovery kinetics of nickel pattern electrode cells, on the other hand, are significantly faster than those of ceria pattern electrode cells. Ceria pattern electrode cells do not recover fully, as shown in Fig. 4. Somewhat superior performance for Ni-GDC cermet anodes compared to Ni-YSZ cermet anodes has been reported in previous studies comparing the two materials [54–57]. This is typically attributed to the MIEC nature of GDC. In the case of a Ni-YSZ, structural changes are observed only on Ni, but in the case of a Ni-GDC, structural changes are observed in the GDC phase [54].

Reduced ceria is expected to react with H_2S forming corresponding sulfides – however, there is a large discrepancy in whether this reaction is expected to proceed in SOFC conditions. It was suggested in [19] that the chemisorption of H_2S on ceria occurs even when it is not thermodynamically favored because of unexpected changes in the gas's local compositions and on the surface. In [19], S removal is observed in the form of breakthrough curves and surface composition mapping. Adsorption and subsequent incorporation into the regions near the surface were proposed for S interaction with ceria [31]. Some cerium oxysulfides are observed by Mai Thi et al. [40]. Thus, selective

chemisorption may lead to the different behavior of ceria when compared to nickel. Although it is anticipated that the ceria will participate in the hydrogen oxidation reaction, it is not postulated that it will completely neutralize the effects of sulfur on cermet anodes. It has been demonstrated that copper/ceria-based anodes are capable of withstanding high temperatures and pollutant concentrations of up to 450 ppm [58]. According to the findings of this investigation, the degradation of the ceria patterns when gold mesh is used has been found to be significant. As a result, in the case of copper, the electronic conductivity of gold is insufficient to compensate. In the case of hydrogen oxidation, it is unlikely that either gold or copper will be catalytically active.

Ceria as an anode material for SOFCs has gotten much attention lately, thanks to its MIEC features and studies on sulfur poisoning studies of the material. Density functional theory (DFT) finds that the formation of surface ceria sulfide is thermodynamically favorable at reduced-state ceria (CeO_{2-x}) [41]. In addition, it is projected that the activation barrier for doped ceria (-lanthanum and -terbia) sulfidation will be lower than that for undoped ceria. The sulfur capacity will grow as the partial pressure of oxygen lowers and the temperature rises. This is used extensively in gas cleaning units. There have been conflicting reports about the tolerance of ceria to sulfur and the formation of sulfides. An equilibrium calculation with FactSage [59] shows that sulfides may form at conditions used in this study (4.6×10^{-6} of sulfur species per mole of Ce_2O_3), and recent work has shown the formation of sulfides [40].

On the other hand, many previous investigations have concluded that the formation of bulk cerium sulfides is unlikely to occur at the temperatures and concentrations used in this work [3,19,60]. While some studies have reported improved tolerance with ceria, it is not usually considered to be any better performing than a nickel as an anode when exposed to H_2S-rich gas [3,19,51]. In any case, the presence of H_2S has a significant poisoning effect on ceria.

Lohsoontorn et al. [3] found that ceria bulk sulfides are not formed at concentrations up to 100 ppm H_2S; nonetheless, changes in local composition can lead to the development of sulfides in some cases. According to Mirfakharaei et al. [45], GDC anode performance declines when exposed to 10 ppm H_2S concentration, with only a partial recovery observed after H_2S was withdrawn from the fuel stream. They did, however, report that utilizing Ni-infiltrated GDC anodes resulted in a significant increase in H_2S tolerance. When Cu-CeO_2-YSZ anodes were used in conjunction with H_2 contaminated fuel, He et al. [58] demonstrated high sulfur tolerance and found that there was no effect on the anode performance at 800 ℃ under 450 ppm sulfur. It is believed that the adsorption of sulfur compounds at the TPB results in a loss of active sites at the TPB and a change of surface characteristics in the case of nickel anode poisoning [8–11,43]. A further possibility for sulfide formation is that it will affect ceria's oxide transport mechanism and redox chemistry, changing its MIEC properties and potentially diminishing the effective active zone [61]. Other studies have also suggested that the GDC phase is associated with increased H_2S tolerance [57].

We find that a rise in polarization resistance occurs primarily at low frequencies, even for pattern electrode cells, which is consistent with our previous findings. In our previous studies [36,37], where the model was developed for hydrogen oxidation on ceria, the low-frequency process was attributed to the electrochemical process, including adsorption, charge transfer, and desorption. Even if sulfur does not participate in the charge transfer process, it is possible to link an increase in polarization resistance to the adsorption of sulfur species on ceria even if sulfur does not participate in charge transfer. The same is simulated in the following section.

3.1.4. *Elementary kinetic modeling of ceria cell*

In this section, we undertake elementary kinetic modeling of H_2S poisoning of ceria pattern electrode cells to develop an approach to quantify the effect of contaminants from microscopic experiments like these and use them in macroscopic simulations. The base model with pure hydrogen oxidation is based on the reaction scheme published previously [37]. Due to limited knowledge about sulfur interaction with ceria-based SOFC anodes, we assume that (i) sulfur does not electrochemically oxidize under reducing conditions, and (ii) sulfur does not chemically react with ceria to form cerium sulfides. These assumptions make the proposed model very preliminary in its nature, and it follows that merely sulfur adsorption at the ceria surface is responsible for the increase in polarization resistance. The sulfur atoms have a strong affinity for oxide-ion sites compared to cerium sites, making sulfur thermodynamically favorable for adsorption on oxide-ion sites instead of cerium sites, as witnessed in several studies [62,63]. Therefore, reaction (5) is added. The overall reaction for hydrogen electrochemical oxidation on ceria can be written as (Kroger-Vink notation):

$$H_2(g) + 2O_o^x + 2Ce_{ce}^x \leftrightarrow H_2O(g) + V_o^{\bullet\bullet} + 2Ce'_{ce} \quad (1)$$

The multistep mechanism for hydrogen oxidation and H_2S poisoning is thus written as

$$H_2(g) + 2O_o^x + 2Ce_{ce}^x \leftrightarrow 2OH_o^{\bullet} + 2Ce'_{ce} \quad (2)$$

$$2OH_o^{\bullet} \leftrightarrow H_2O(g) + V_o^{\bullet\bullet} + O_o^x \quad (3)$$

$$V_o^{\bullet\bullet}(surf) + O_o^x(sub) \leftrightarrow V_o^{\bullet\bullet}(sub) + O_o^x(surf) \quad (4)$$

$$H_2S(g) + O_o^x \leftrightarrow H_2O(g) + S_o^x \quad (5)$$

The subscripts "o" and "ce" refer to the anionic and cationic sites in the crystal lattice, respectively, and the superscripts refer to the effective charge. This implies that O_o^x is a neutral oxide anion, $V_o^{\bullet\bullet}$ is an oxide-ion vacancy with an effective charge of 2+, Ce_{ce}^x is a neutral cerium cation and Ce'_{ce} is a localized electron at cerium (Ce^{3+}). Correspondingly, $OH_o^{\bullet}$ and S_o^x are hydroxyl, and sulfur ions residing at anionic sites, respectively. In line with the previous findings [36,37], reaction (2) is the rate-determining step. The above scheme exhibits a global interaction of sulfur with ceria with an assumption that $OH_o^{\bullet}$ and S_o^x do not diffuse into the bulk.

The impedance spectra for electrochemical hydrogen oxidation before sulfur contamination are simulated first using thermodynamic and kinetic parameters reported previously [37]. Then the effect of sulfur contaminant on the impedance spectra is simulated using activation energy (= 16 kJ/mol) and H_2S reaction order (= 0.38 kJ/mol) as given in [62]. The pre-exponent factor for reaction (5) is considered a

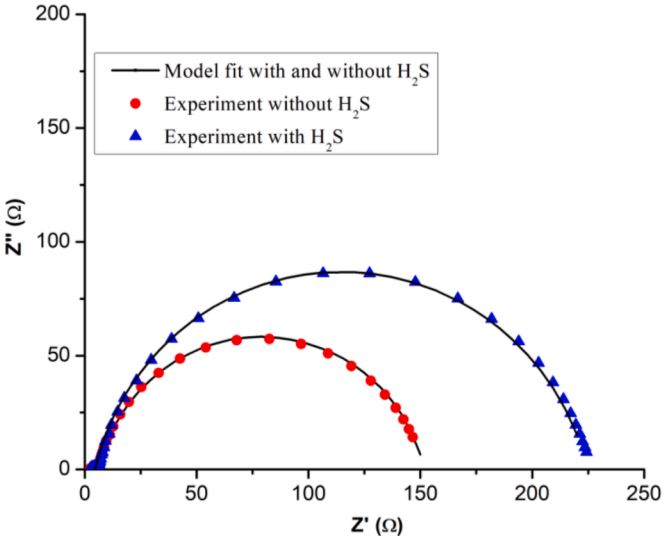

Fig. 5. Model fitting and experimental data of H_2 oxidation on ceria without and with 20 ppm H_2S at 850 ℃.

free fit parameter to match the experimental impedance spectra. Fig. 5 shows the experimental and simulated spectra for electrochemical hydrogen oxidation without and with 20 ppm H_2S contaminant at 850 ℃. The obtained coverages of oxide-ion species have been discussed in detail previously [37] but are presented here in Table 1 for Comparison with H_2S poisoning.

The best fit value of the pre-exponent factor of the forward rate constant of reaction (5) is found to be 4.45×10^{-4} mol/cm^2.sec. The fractional surface coverages, as shown in Table 1, also compare well with [64], where surface coverages found by XPS were 0.6–0.7 for O_o^x and 0.1–0.2 for $OH_o^\bullet$ albeit at 700 ℃ in their case. When comparing surface coverages with and without poisoning, sulfur adsorption is found to be a significant factor in influencing the response to the poisoning. The kinetics of this reaction scheme is slower, and the resultant current density is lower. It is important to note that the proposed model has considered only surface adsorption of sulfur atoms at oxide-ion sites, whereas sulfur electrochemical oxidation and formation of ceria sulfides have been ignored. Therefore the model can only capture the reversible performance loss. The kinetics obtained using competitive interaction mechanisms may differ from the model considered here. Therefore further refinement of the model is suggested to capture the effect of reversible and irreversible performance loss.

3.2. Effect of HCl contaminant on nickel and ceria cells

3.2.1. Effect on cell performance

The impedance spectra of pattern electrode cells before HCl exposure, with 60 ppm and 150 ppm HCl, and after removal of HCl from the gas stream are shown in Fig. 6. The corresponding bode plots are given in the supplementary material (Figs. S5 and S6). It may be noted that the polarization resistance reduces when HCl is added to the hydrogen gas, which is true for both nickel and ceria pattern electrode cells. At 830 ℃, the polarization resistance of nickel pattern electrode cells contaminated by 60 ppm and 150 ppm HCl is lower than the pre-contamination polarization resistance by a factor of 1.50 and 1.82, respectively. Similar is the case with the ceria pattern electrode cell. This observation is unintuitive and has not been reported previously. To the best of the authors' knowledge, pattern electrode cells have never been tested in an HCl environment, so no direct comparison can be made. Otherwise, in relevant studies conducted with cermet cells, no or insignificant effect on the cell performance has been reported for HCl concentration below 50 ppm [13–15,30,65,66]. Both reversible [16,17] and permanent [18] performance loss have been reported at higher concentrations.

Further, after removing HCl from the gas stream, the impedance spectra did not completely recover to the pre-contamination value, at least in this study's test duration (> 20 h). Rather, the polarization resistance was recorded lower for the nickel pattern electrode cell (~18.9 %) and higher for the ceria pattern electrode cell (~7.5 %) than the pre-contamination value. Therefore, the HCl treatment of both materials leaves permanent footprints on the cell performance.

Since no literature comparison could be made for pattern electrode cell results, we thereby tested the effect of HCl on symmetrical Ni/GDC cermet cells obtained from HC Starck/Kerafol, and the results are shown in Fig. 7. As can be observed, 60 ppm HCl does not affect cell performance, and this observation aligns with the findings of our recent experiments conducted with electrolyte-supported 10×10 cm Ni/GDC cells using 50 ppm HCl [15]. However, the higher concentration leads to a reversible increase in the cell polarization resistance - the polarization resistance increased by 25 % at 300 ppm, consistent with the previous results [13,18].

Table 1
Fractional coverage of oxide-site species without and with 20 ppm H_2S exposure at 850 ℃.

Coverage	Without H_2S	With H_2S
O_o^x	0.788	0.624
$OH_o^\bullet$	0.127	0.120
S_o^x	–	0.188

3.2.2. Discussion on HCl contamination

Electrochemical measurements show that the polarization resistance of pattern electrode cells drops upon adding HCl gas to the hydrogen gas stream. The polarization resistance of Ni/GDC cermet cells, on the other hand, remains unaffected at HCl concentrations up to 60 ppm and reversibly increases at higher concentrations. When exposed to high HCl concentrations, the deposited Cl species on the catalyst surface were responsible for the performance degradation found in prior investigations with Ni/YSZ and Ni/GDC cermet electrodes. The mechanism is referred to as adsorption-types poisoning [67]. This adsorption can be analyzed separately from nickel and ceria catalysts' perceptive. The dissociative adsorption of HCl on a nickel surface can be represented as the following:

$$HCl_{(g)} + A_{Ni} \leftrightarrow Cl_{Ni} + \frac{1}{2}H_2 \quad (2a)$$

A_{Ni} is a free adsorption site at the nickel surface, and Cl_{Ni} is the corresponding adsorbed chlorine specie. Cl_{Ni} binds to nickel's free surface sites, reducing the number of sites accessible for hydrogen adsorption. As a result, the cell's performance should deteriorate, as indicated in [16–18]. Nickel pattern electrode cells, on the other hand, demonstrated superior cell performance at all HCl concentrations tested in this study. Alternately, sublimation-types poisoning is also responsible for cell performance degradation in which HCl reacts with a nickel catalyst and forms gaseous $NiCl_2$ as:

$$2HCl + Ni \leftrightarrow NiCl_{2(g)} + H_2 \quad (3a)$$

During the redox reactions, gaseous $NiCl_2$ escapes from the anode surface and reduces the nickel/YSZ ratio of the cermet, finally leading to the permanent deterioration [67]. Our equilibrium calculation (shown in the supplementary information Fig. S7) using FactSage software [59] shows that the gas phase activity of $NiCl_2$ (g) at 800 ℃ is of the order of 10^{-14}, is significantly small, and cannot result in any noticeable difference in the performance. Neither an increase in polarization resistance after adding HCl to wet H_2 gas nor a persistent rise in polarization resistance after removing HCl from the gas stream was observed in our experiments. Instead, a reduction in resistance is observed, which cannot be explained by adsorption or sublimation type interactions.

Electrochemical reactions are thought to occur at the TPB between nickel, YSZ, and gas phases on nickel cells. Because of this, cell performance is improved when the TPB length is increased. According to the results of pattern electrode cell studies, the thermal and redox treatment of the cell can potentially damage the electrode layer, increasing TPB length. Morphological changes in the pattern surface have been observed in our post-test SEM analysis. It is unclear whether HCl plays a critical role in degrading the interface or washing off any impurities that have segregated at the TPB. Many previous studies examining the synergistic effect of various coal contaminants on the performance of Ni/YSZ anode-based SOFCs have discovered that the presence of Cl species can alleviate the performance loss caused by other contaminants such as arsenic and phosphorus [68,69].

Like nickel pattern electrode cells, Ceria pattern electrode cells have been demonstrated to exhibit decreased polarization resistance when exposed to HCl. Ceria, while a promising catalyst for the production of Cl_2 gas under Deacon conditions (350–450°C and O_2 /HCl = 1), forms a chlorinated phase when exposed to a sub-stoichiometric environment (O_2 /HCl = 0.25), and this chlorinated phase can lead to a reversible catalyst deactivation [70]. Because only traces of chlorine were discovered in the EDS analysis performed in this work, the formation of chlorinated cerium may be ruled out as a possibility (shown in Fig. S8). Furthermore, as shown in the supplementary information (Figs. S7 and S9), the activities of $CeCl_3$ in the gaseous and solid phases at 800°C are

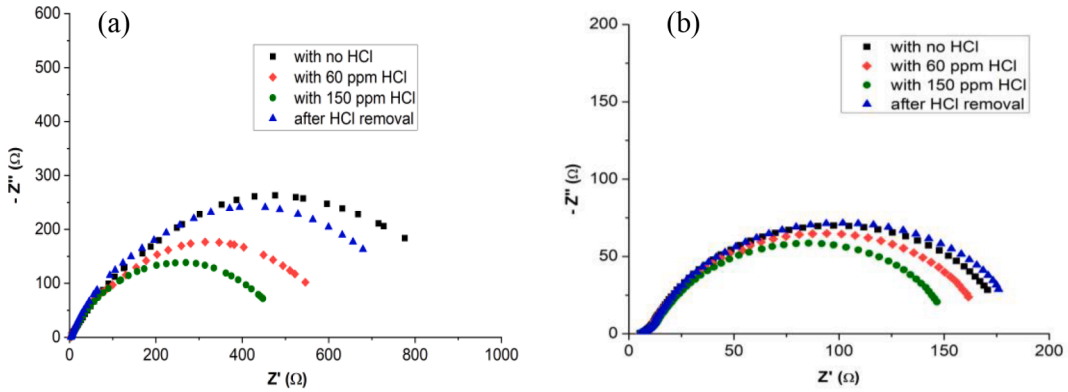

Fig. 6. Impedance spectra of HCl contamination of pattern electrode cells of nickel (a) and ceria (b) at 830 °C.

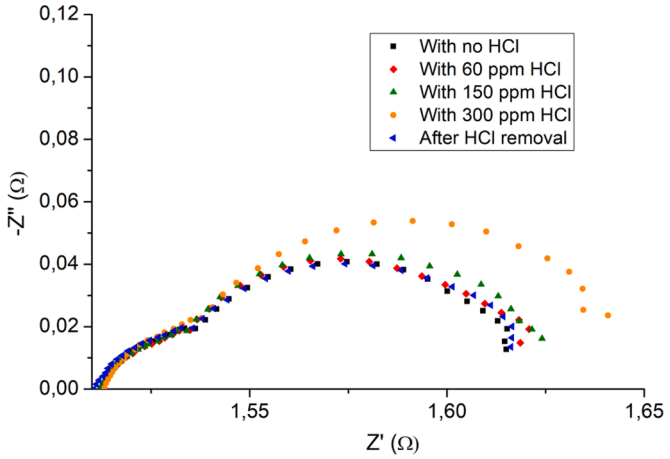

Fig. 7. Impedance spectra of HCl contamination of nickel/GDC cermet cell at 800 °C.

far too low to cause any considerable loss of cerium. Contrary to our observations, the polarization resistance should increase even if ceria chlorination happens. The ceria pattern had deteriorated in the SEM image, which was not predicted to occur due to the HCl treatment because the cell performance was shown to be largely reversible when the HCl was added and removed. Unlike pattern electrode cells, Ni/GDC cermet cell performance remains unaffected at lower HCl concentrations (up to 60 ppm). The decrease in the polarization resistance of nickel and ceria pattern electrode cells possibly points towards the facilitating role of HCl for electrochemical hydrogen oxidation, and more specifically, the charge transfer step as the charge transfer step is the rate-determining in the oxidation process [35,37]. The same has not been observed in the Ni/GDC cermet cell case because the charge transfer resistance of the Ni/GDC electrode is generally small compared to the resistance offered by surface and gas-phase processes.

However, even though pattern electrode cells exhibit a decrease in polarization resistance, the data found with Ni/GDC cermet electrode cells are consistent with the previously described trend in the literature [13,18]. Compared to the pattern electrode, the number of active sites in the cermet electrode is substantially higher, which may explain why the resistance from the TPB-related activity may be minimal compared to the resistance from other physicochemical processes in the electrode. Maybe this explains why, in contrast to pattern electrode cells, there is no influence of HCl on the performance of the cermet cell at low concentrations. Because of a lack of understanding of the electrochemistry of the Ni/GDC anode, it is difficult to establish a mechanistic relationship between the interaction of HCl with Ni/GDC and other materials. The observed effect of HCl on the anode electrochemistry will be further examined and discussed in our next paper.

4. Conclusions

Pattern electrode cells of nickel and ceria were prepared, and the effect of H_2S and HCl on their performance was tested using electrochemical impedance spectroscopy. When H_2S was introduced into the system, it was discovered that the polarization resistance of both nickel and ceria pattern electrode cells increased significantly, as previously reported. After removing H_2S, the change is found completely reversible for nickel and only partially reversible for ceria. We have observed that the kinetics of poisoning nickel and ceria pattern electrode cells is faster than the kinetics of recovery from poisoning. Only the nickel pattern electrode cells, on the other hand, recover rapidly and within a period of time comparable to that required for the poisoning. After the H_2S has been removed from the ceria pattern electrode cells, it takes a very long time for them to stabilize. The findings of these experiments indicate that H_2S has a significant effect on the ceria surface structure. However, while it was hard to determine the species causing the anode poisoning, some of the adsorption is irreversible or at least difficult to reverse.

A model with elementary kinetics for H_2S adsorption on ceria was also made, assuming that the adsorbed species are not involved in the charge transfer process. It has been observed that the surface coverage of the S species is substantial, which inhibits the adsorption of H and the subsequent oxidation of ceria on the surface. Even though this is not a detailed model, it is likely to reflect the reversible influence of H_2S on the polarization resistance. The model can further be refined to incorporate sulfur participation in the charge transfer process and address irreversible cell degradation.

When tested with the HCl contaminant, both nickel and ceria pattern electrode cells show a decrease in cell polarization resistance, unlike the H_2S contaminant, where an increase in the resistance was observed. The underlying mechanism for such behavior remains inconclusive and requires further investigation. However, the Ni/GDC cermet cell did not change the polarization resistance up to 60 ppm HCl concentration, consistent with the literature. A higher concentration of HCl (150 and 300 ppm) resulted in a recoverable performance loss.

CRediT authorship contribution statement

A.N. Tabish: Methodology, Investigation, Visualization, Writing – original draft. **H.C. Patel:** Methodology, Investigation, Writing – original draft. **A. Mani:** Writing – review & editing. **J. Schoonman:** . **P.V. Aravind:** Writing – review & editing.

Declaration of Competing Interest

The authors declare that they have no known competing financial interests or personal relationships that could have appeared to influence

the work reported in this paper.

Supplementary materials

Supplementary material associated with this article can be found, in the online version, at doi:10.1016/j.electacta.2022.140592.

References

[1] M.J. Escudero, J.L. Serrano, Individual impact of several impurities on the performance of direct internal reforming biogas solid oxide fuel cell using W-Ni-CeO_2 as anode, Int. J. Hydrog. Energy 44 (2019) 20616–20631, https://doi.org/10.1016/j.ijhydene.2019.06.028.

[2] M. Singh, D. Zappa, E. Comini, Solid oxide fuel cell: decade of progress, future perspectives and challenges, Int. J. Hydrog. Energy 46 (2021) 27643–27674, https://doi.org/10.1016/j.ijhydene.2021.06.020.

[3] P. Lohsoontorn, D.J.L. Brett, N.P. Brandon, Thermodynamic predictions of the impact of fuel composition on the propensity of sulphur to interact with Ni and ceria-based anodes for solid oxide fuel cells, J. Power Sources 175 (2008) 60–67, https://doi.org/10.1016/j.jpowsour.2007.09.065.

[4] A. Norheim, I. Wærnhus, M. Broström, J.E. Hustad, A. Vik, Experimental studies on the influence of H2S on solid oxide fuel cell performance at 800°C, Energy Fuels 21 (2007) 1098–1101, https://doi.org/10.1021/ef060532m.

[5] J. Kupecki, D. Papurello, A. Lanzini, Y. Naumovich, K. Motylinski, M. Blesznowski, M. Santarelli, Numerical model of planar anode supported solid oxide fuel cell fed with fuel containing H2S operated in direct internal reforming mode (DIR-SOFC), Appl. Energy 230 (2018) 1573–1584, https://doi.org/10.1016/j.apenergy.2018.09.092.

[6] W.A. Maza, E.D. Pomeroy, D.A. Steinhurst, R.A. Walker, J.C. Owrutsky, Operando optical studies of sulfur contamination in syngas operation of solid oxide fuel cells, J. Power Sources 510 (2021), 230398, https://doi.org/10.1016/j.jpowsour.2021.230398.

[7] Y. Matsuzaki, I. Yasuda, Poisoning effect of sulfur-containing impurity gas on a SOFC anode: part I. Dependence on temperature, time, and impurity concentration, Solid State Ion. 132 (2000) 261–269, https://doi.org/10.1016/s0167-2738(00)00653-6.

[8] Z. Cheng, J.H. Wang, Y. Choi, L. Yang, M.C. Lin, M. Liu, From Ni-YSZ to sulfur-tolerant anode materials for SOFCs: electrochemical behavior, *in situ* characterization, modeling, and future perspectives, Energy Environ. Sci. 4 (2011) 4380–4409, https://doi.org/10.1039/c1ee01758f.

[9] E. Brightman, D.G. Ivey, D.J.L. Brett, N.P. Brandon, The effect of current density on H_2S-poisoning of nickel-based solid oxide fuel cell anodes, J. Power Sources, (2011) 7182–7187, https://doi.org/10.1016/j.jpowsour.2010.09.089.

[10] A. Hagen, G.B. Johnson, P. Hjalmarsson, Electrochemical evaluation of sulfur poisoning in a methane-fuelled solid oxide fuel cell: effect of current density and sulfur concentration, J. Power Sources 272 (2014) 776–785, https://doi.org/10.1016/j.jpowsour.2014.08.125.

[11] H.H. Mai Thi, N. Rosman, N. Sergent, T. Pagnier, Impedance and Raman spectroscopy study of effect of H2S on Ni-YSZ SOFC anodes, Fuel Cells 17 (2017) 367–377, https://doi.org/10.1002/fuce.201600182.

[12] H.S. Lee, H.M. Lee, J.Y. Park, H.T. Lim, Degradation behavior of Ni-YSZ anode-supported solid oxide fuel cell (SOFC) as a function of H2S concentration, Int. J. Hydrog. Energy 43 (2018) 22511–22518, https://doi.org/10.1016/j.ijhydene.2018.09.189.

[13] H. Madi, A. Lanzini, D. Papurello, S. Diethelm, C. Ludwig, M. Santarelli, J. Van herle, Solid oxide fuel cell anode degradation by the effect of hydrogen chloride in stack and single cell environments, J. Power Sources 326 (2016) 349–356, https://doi.org/10.1016/j.jpowsour.2016.07.003.

[14] T.S. Li, C. Xu, T. Chen, H. Miao, W.G. Wang, Chlorine contaminants poisoning of solid oxide fuel cells, J. Solid State Electrochem. 15 (2011) 1077–1085, https://doi.org/10.1007/s10008-010-1166-x.

[15] A. Cavalli, R. Bernardini, T. Del Carlo, P.V. Aravind, Effect of H2S and HCl on solid oxide fuel cells fed with simulated biosyngas containing primary tar, Energy Sci. Eng. 7 (2019) 2456–2468, https://doi.org/10.1002/ese3.434.

[16] J.P. Trembly, R.S. Gemmen, D.J. Bayless, The effect of coal syngas containing HCl on the performance of solid oxide fuel cells: Investigations into the effect of operational temperature and HCl concentration, J. Power Sources 169 (2007) 347–354, https://doi.org/10.1016/j.jpowsour.2007.03.018.

[17] O.A. Marina, L.R. Pederson, E.C. Thomsen, C.A. Coyle, K.J. Yoon, Reversible poisoning of nickel/zirconia solid oxide fuel cell anodes by hydrogen chloride in coal gas, J. Power Sources 195 (2010) 7033–7037, https://doi.org/10.1016/j.jpowsour.2010.05.006.

[18] C. Xu, M. Gong, J.W. Zondlo, X.B. Liu, H.O. Finklea, The effect of HCl in syngas on Ni-YSZ anode-supported solid oxide fuel cells, J. Power Sources 195 (2010) 2149–2158, https://doi.org/10.1016/j.jpowsour.2009.09.079.

[19] Z. Cheng, M. Liu, Rational design of sulfur-tolerant anode materials for solid oxide fuel cells, ECS Trans. (2013) 217–229, https://doi.org/10.1149/05802.0217ecst.

[20] S. Li, Z. Lu, Z. Yang, X. Chu, Y. Zhang, D. Ma, The sulfur tolerance mechanism of the Cu/CeO_2 system, Int. J. Hydrog. Energy 39 (2014) 1957–1966, https://doi.org/10.1016/j.ijhydene.2013.11.132.

[21] M.J. Escudero, A. Fuerte, Electrochemical analysis of a system based on W and Ni combined with CeO_2 as potential sulfur-tolerant SOFC anode, Fuel Cells 16 (2016) 340–348, https://doi.org/10.1002/fuce.201500076.

[22] C.J. Laycock, J.Z. Staniforth, R.M. Ormerod, Biogas as a fuel for solid oxide fuel cells and synthesis gas production: effects of ceria-doping and hydrogen sulfide on the performance of nickel-based anode materials, Dalton Trans. 40 (2011) 5494–5504, https://doi.org/10.1039/c0dt01373k.

[23] M.T. Mehran, M.Z. Khan, S.B. Lee, T.H. Lim, S. Park, R.H. Song, Improving sulfur tolerance of Ni-YSZ anodes of solid oxide fuel cells by optimization of microstructure and operating conditions, Int. J. Hydrog. Energy 43 (2018) 11202–11213, https://doi.org/10.1016/j.ijhydene.2018.04.200.

[24] G. Pongratz, V. Subotić, H. Schroettner, C. Hochenauer, M. Skrzypkiewicz, J. Kupecki, A. Anca-Couce, R. Scharler, Analysis of H2S-related short-term degradation and regeneration of anode- and electrolyte supported solid oxide fuel cells fueled with biomass steam gasifier product gas, Energy (2021) 218, https://doi.org/10.1016/j.energy.2020.119556.

[25] X. Hu, J. Dong, A novel study of sulfur-absorption via samarium-doped cerium sorbent at high temperature, J. Rare Earths 38 (2020) 617–624, https://doi.org/10.1016/j.jre.2020.03.006.

[26] D. Liu, W. Zhou, J. Wu, CeO_2-MnOx/ZSM-5 sorbents for H2S removal at high temperature, Chem. Eng. J. 284 (2016) 862–871, https://doi.org/10.1016/j.cej.2015.09.028.

[27] K. Svoboda, J. Leitner, J. Havlica, M. Hartman, M. Pohořelý, J. Brynda, M. Šyc, Y. P. Chyou, P.C. Chen, Thermodynamic aspects of gasification derived syngas desulfurization, removal of hydrogen halides and regeneration of spent sorbents based on La2O3/La2O2CO3 and cerium oxides, Fuel 197 (2017) 277–289, https://doi.org/10.1016/j.fuel.2016.12.035.

[28] C. Li, F. Hess, I. Djerdj, G. Chai, Y. Sun, Y. Guo, B.M. Smarsly, H. Over, The stabilizing effect of water and high reaction temperatures on the CeO_2-catalyst in the harsh HCl oxidation reaction, J. Catal. 357 (2018) 257–262, https://doi.org/10.1016/j.jcat.2017.11.019.

[29] G. Jeanmonod, S. Diethelm, J. Van herle, Poisoning effects of chlorine on a solid oxide cell operated in co-electrolysis, J. Power Sources 506 (2021), https://doi.org/10.1016/j.jpowsour.2021.230247.

[30] P.V. Aravind, J.P. Ouweltjes, N. Woudstra, G. Rietveld, Impact of biomass-derived contaminants on SOFCs with Ni/gadolinia-doped ceria anodes, Electrochem. Solid State Lett. 11 (2008) B24, https://doi.org/10.1149/1.2820452.

[31] M. Gerstl, A. Nenning, R. Iskandar, V. Rojek-Wöckner, M. Bram, H. Hutter, A. K. Opitz, The sulphur poisoning behaviour of gadolinia doped ceria model systems in reducing atmospheres, Materials 9 (2016), https://doi.org/10.3390/ma9080649.

[32] H. Kurokawa, T.Z. Sholklapper, C.P. Jacobson, L.C. De Jonghe, S.J. Visco, Ceria nanocoating for sulfur tolerant Ni-based anodes of solid oxide fuel cells, Electrochem. Solid-State Lett. 10 (2007) 135–138, https://doi.org/10.1149/1.2748630.

[33] P.V. Aravind, J.P. Ouweltjes, J. Schoonman, Diffusion impedance on nickel/gadolinia-doped ceria anodes for solid oxide fuel cells, J. Electrochem. Soc. 156 (2009) B1417, https://doi.org/10.1149/1.3231490.

[34] H.C. Patel, A.N. Tabish, F. Comelli, P.V. Aravind, Oxidation of H2, CO and syngas mixtures on ceria and nickel pattern anodes, Appl. Energy 154 (2015) 912–920, https://doi.org/10.1016/j.apenergy.2015.05.049.

[35] A.N. Tabish, H.C. Patel, P.V. Aravind, Electrochemical oxidation of syngas on nickel and ceria anodes, Electrochim. Acta 228 (2017) 575–585, https://doi.org/10.1016/j.electacta.2017.01.074.

[36] H.C. Patel, A.N. Tabish, P.V. Aravind, Modelling of elementary kinetics of H2 and CO oxidation on ceria pattern cells, Electrochim. Acta 182 (2015) 202–211, https://doi.org/10.1016/j.electacta.2015.09.027.

[37] A.N. Tabish, H.C. Patel, J. Schoonman, P.V. Aravind, A detailed look into hydrogen electrochemical oxidation on ceria anodes, Electrochim. Acta 283 (2018) 789–797, https://doi.org/10.1016/j.electacta.2018.05.058.

[38] A.N. Tabish, H.C. Patel, P. Chundru, J.N. Stam, P.V. Aravind, An SOFC anode model using TPB-based kinetics, Int. J. Hydrog. Energy 45 (2020) 27563–27574, https://doi.org/10.1016/j.ijhydene.2020.07.037.

[39] A.N. Tabish, L. Fan, I. Farhat, M. Irshad, S.Z. Abbas, Computational fluid dynamics modeling of anode-supported solid oxide fuel cells using triple-phase boundary-based kinetics, J. Power Sources 513 (2021), 230564, https://doi.org/10.1016/j.jpowsour.2021.230564.

[40] H.H. Mai Thi, B. Saubat, N. Sergent, T. Pagnier, *In situ* Raman and optical characterization of H2S reaction with Ni-based anodes for SOFCs, Solid State Ion. 272 (2015) 84–90, https://doi.org/10.1016/j.ssi.2015.01.007.

[41] A.D. Mayernick, R. Li, K.M. Dooley, M.J. Janik, Energetics and mechanism for H_2S adsorption by ceria-lanthanide mixed oxides: Implications for the desulfurization of biomass gasifier effluents, J. Phys. Chem. C 115 (2011) 24178–24188, https://doi.org/10.1021/jp206827n.

[42] D.W. Choi, M. Ohashi, C.A. Lozano, J.W. Vanzee, P. Aungkavattana, S. Shimpalee, Sulfur diffusion of hydrogen sulfide contaminants to cathode in a micro-tubular solid oxide fuel cell, Electrochim. Acta 321 (2019), https://doi.org/10.1016/j.electacta.2019.134713.

[43] Z. Cheng, M. Liu, Characterization of sulfur poisoning of Ni-YSZ anodes for solid oxide fuel cells using *in situ* Raman microspectroscopy, Solid State Ion. 178 (2007) 925–935, https://doi.org/10.1016/j.ssi.2007.04.004.

[44] A. Lussier, S. Sofie, J. Dvorak, Y.U. Idzerda, Mechanism for SOFC anode degradation from hydrogen sulfide exposure, Int. J. Hydrog. Energy 33 (2008) 3945–3951, https://doi.org/10.1016/j.ijhydene.2007.11.033.

[45] B. Mirfakhraei, S. Paulson, V. Thangadurai, V. Birss, Enhanced hydrogen oxidation activity and H2S tolerance of Ni-infiltrated ceria solid oxide fuel cell anodes, J. Power Sources 243 (2013) 95–101, https://doi.org/10.1016/j.jpowsour.2013.05.150.

[46] M. Riegraf, V. Yurkiv, R. Costa, G. Schiller, K.A. Friedrich, Evaluation of the effect of sulfur on the performance of nickel/gadolinium-doped ceria based solid oxide fuel cell anodes, ChemSusChem 10 (2017) 587–599, https://doi.org/10.1002/cssc.201601320.
[47] D. Papurello, A. Lanzini, S. Fiorilli, F. Smeacetto, R. Singh, M. Santarelli, Sulfur poisoning in Ni-anode solid oxide fuel cells (SOFCs): deactivation in single cells and a stack, Chem. Eng. J. 283 (2016) 1224–1233, https://doi.org/10.1016/j.cej.2015.08.091.
[48] J.F.B. Rasmussen, A. Hagen, The effect of H2S on the performance of Ni-YSZ anodes in solid oxide fuel cells, J. Power Sources 191 (2009) 534–541, https://doi.org/10.1016/j.jpowsour.2009.02.001.
[49] M. Gong, X. Liu, J. Trembly, C. Johnson, Sulfur-tolerant anode materials for solid oxide fuel cell application, J. Power Sources 168 (2007) 289–298, https://doi.org/10.1016/j.jpowsour.2007.03.026.
[50] S. Zha, Z. Cheng, M. Liu, Sulfur poisoning and regeneration of Ni-based anodes in solid oxide fuel cells, J. Electrochem. Soc. 154 (2007) B201, https://doi.org/10.1149/1.2404779.
[51] B. Mirfakhraei, V.I. Birss, V. Thangadurai, S. Paulson, K.E. Béré, F. Gitzhofer, Electrochemical performance and H 2 S poisoning study of Mo-doped ceria (CMO) SOFC anodes, ECS Trans. 35 (2019) 1727–1734, https://doi.org/10.1149/1.3570160.
[52] J. Nielsen, B.R. Sudireddy, A. Hagen, Å.H. Persson, Performance factors and sulfur tolerance of metal supported solid oxide fuel cells with nanostructured Ni:GDC infiltrated anodes, J. Electrochem. Soc. 163 (2016) F574–F580, https://doi.org/10.1149/2.1081606jes.
[53] G. Nurk, T. Huthwelker, A. Braun, C. Ludwig, E. Lust, R.P.W.J. Struis, Redox dynamics of sulphur with Ni/GDC anode during SOFC operation at mid- and low-range temperatures: an operando S K-edge XANES study, J. Power Sources 240 (2013) 448–457, https://doi.org/10.1016/j.jpowsour.2013.03.187.
[54] L. Zhang, S.P. Jiang, H.Q. He, X. Chen, J. Ma, X.C. Song, A comparative study of H2S poisoning on electrode behavior of Ni/YSZ and Ni/GDC anodes of solid oxide fuel cells, Int. J. Hydrog. Energy 35 (2010) 12359–12368, https://doi.org/10.1016/j.ijhydene.2010.08.067.
[55] M. Riegraf, A. Zekri, M. Knipper, R. Costa, G. Schiller, K.A. Friedrich, Sulfur poisoning of Ni/Gadolinium-doped ceria anodes: a long-term study outlining stable solid oxide fuel cell operation, J. Power Sources 380 (2018) 26–36, https://doi.org/10.1016/j.jpowsour.2018.01.067.
[56] S. Kavurucu Schubert, M. Kusnezoff, A. Michaelis, S.I. Bredikhin, Comparison of the performances of single cell solid oxide fuel cell stacks with Ni/8YSZ and Ni/10CGO anodes with H 2S containing fuel, J. Power Sources 217 (2012) 364–372, https://doi.org/10.1016/j.jpowsour.2012.06.020.
[57] A.I. Marquez, T.R. Ohrn, J.P. Trembly, D.C. Ingram, D.J. Bayless, Effects of coal syngas and H2S on the performance of solid oxide fuel cells. Part 2. Stack tests, J. Power Sources 164 (2007) 659–667, https://doi.org/10.1016/j.jpowsour.2006.10.102.
[58] H. He, R.J. Gorte, J.M. Vohs, Highly sulfur tolerant Cu-ceria anodes for SOFCs, Electrochem. Solid-State Lett. 8 (2005), https://doi.org/10.1149/1.1896469.
[59] C.W. Bale, P. Chartrand, S.A. Degterov, G. Eriksson, K. Hack, R. Ben Mahfoud, J. Melançon, A.D. Pelton, S. Petersen, FactSage thermochemical software and databases, Calphad 26 (2002) 189–228, https://doi.org/10.1016/S0364-5916(02)00035-4. Computer Coupling of Phase Diagrams and Thermochemistry.
[60] J. Sugimoto, T. Kawabata, Y. Shiratori, S. Taniguchi, K. Sasaki, Effect of ceria addition in SOFC anodes on sulfur poisoning, ECS Trans. 57 (2013) 1395–1400, https://doi.org/10.1149/05701.1395ecst.
[61] P.K. Cheekatamarla, A.M. Lane, Catalytic autothermal reforming of diesel fuel for hydrogen generation in fuel cells: II. Catalyst poisoning and characterization studies, J. Power Sources 154 (2006) 223–231, https://doi.org/10.1016/j.jpowsour.2005.04.011.
[62] M. Kobayashi, M. Flytzani-Stephanopoulos, Reduction and sulfidation kinetics of cerium oxide and Cu-modified cerium oxide, Ind. Eng. Chem. Res. 41 (2002) 3115–3123, https://doi.org/10.1021/ie010815w.
[63] M.A. Ocsachoque, J.I. Eugenio Russman, B. Irigoyen, D. Gazzoli, M.G. González, Experimental and theoretical study about sulfur deactivation of Ni/CeO_2 and Rh/CeO_2 catalysts, Mater. Chem. Phys. 172 (2016) 69–76, https://doi.org/10.1016/j.matchemphys.2015.12.062.
[64] C. Zhang, Y. Yu, M.E. Grass, C. Dejoie, W. Ding, K. Gaskell, N. Jabeen, Y.P. Hong, A. Shavorskiy, H. Bluhm, W.X. Li, G.S. Jackson, Z. Hussain, Z. Liu, B.W. Eichhorn, Mechanistic studies of water electrolysis and hydrogen electro-oxidation on high temperature ceria-based solid oxide electrochemical cells, J. Am. Chem. Soc. 135 (2013) 11572–11579, https://doi.org/10.1021/ja402604u.
[65] J.E. Bao, G.N. Krishnan, P. Jayaweera, J. Perez-Mariano, A. Sanjurjo, Effect of various coal contaminants on the performance of solid oxide fuel cells: part I. Accelerated testing, J. Power Sources 193 (2009) 607–616, https://doi.org/10.1016/j.jpowsour.2009.04.034.
[66] G. Buchinger, P. Hinterreiter, T. Raab, S. Griesser, R. Claassen, D.P. Claassen, W. Sitte, D. Meissner, Operating microtubular SOFCS with hydrogen chloride and hydrogen sulfide containing fuels and synthetic wood gas, J. Fuel Cell Sci. Technol. 3 (2006) 280–283, https://doi.org/10.1115/1.2205361.
[67] K. Haga, Y. Shiratori, K. Ito, K. Sasaki, Chlorine poisoning of SOFC Ni-cermet anodes, J. Electrochem. Soc. 155 (2008) B1233, https://doi.org/10.1149/1.2980521.
[68] J. Bao, G.N. Krishnan, P. Jayaweera, A. Sanjurjo, Impedance study of the synergistic effects of coal contaminants: is Cl a contaminant or a performance stabilizer? J. Electrochem. Soc. 157 (2010) B415, https://doi.org/10.1149/1.3291913.
[69] J.E. Bao, G.N. Krishnan, P. Jayaweera, A. Sanjurjo, Effect of various coal gas contaminants on the performance of solid oxide fuel cells: part III. Synergistic effects, J. Power Sources 195 (2010) 1316–1324, https://doi.org/10.1016/j.jpowsour.2009.09.018.
[70] A.P. Amrute, C. Mondelli, M. Moser, G. Novell-Leruth, N. López, D. Rosenthal, R. Farra, M.E. Schuster, D. Teschner, T. Schmidt, J. Pérez-ramírez, Performance, structure, and mechanism of CeO_2 in HCl oxidation to Cl_2, J. Catal. 286 (2012) 287–297, https://doi.org/10.1016/j.jcat.2011.11.016.